Manipulating the Growth Kinetics of Vapor-Liquid-Solid Propagated Ge Nanowires

Subhajit Biswas, Colm O'Regan, Nikolay Petkov, Michael A. Morris

and Justin D. Holmes[*]

Materials Chemistry & Analysis Group, Department of Chemistry and the Tyndall National Institute, University College Cork, Cork, Ireland. Centre for Research on Adaptive Nanostructures and Nanodevices (CRANN), Trinity College Dublin, Dublin 2, Ireland.

RECEIVED DATE (to be automatically inserted after your manuscript is accepted if required according to the journal that you are submitting your paper to)

*To whom correspondence should be addressed: Tel: +353 (0)21 4903608; Fax: +353 (0)21 4274097; E-mail: j.holmes@ucc.ie

Table of Content Graphic:

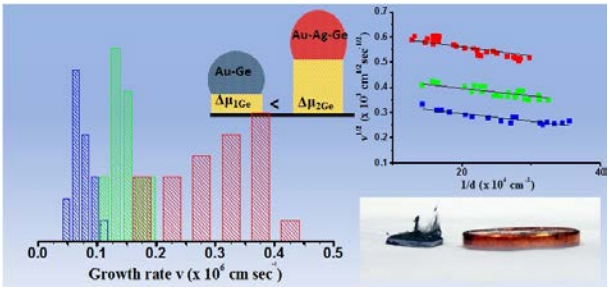

ABSTRACT. This article describes an innovative approach in which bimetallic alloy seeds of Au_xAg_{1-x} are used to enhance the growth kinetics of Ge nanowires, via a vapor-liquid-solid (VLS) growth technique. The decreased equilibrium concentration and increased supersaturation of Ge in the liquid alloy seeds, compared to pure Au seeds, results in favorably growth kinetics and the realization of high-aspect ratio millimetre-long Ge nanowires. Also detailed is the manifestation of the Gibbs-Thomson effect resulting in diameter-dependent nanowire growth rates as a function of the Au-Ag-Ge eutectic composition. Significantly, Au_xAg_{1-x} alloy seeds lower the *critical diameter* of the Ge nanowires in this liquid-seeded growth approach. In-situ TEM heating experiments established the correlation between the growth kinetics and equilibrium eutectic compositions in the ternary growth systems. The fundamental insights of nanowire growth demonstrated with the ternary eutectic alloys opens up opportunities to engineer the aspect ratio and morphology of a range of semiconductor nanowires.

KEYWORDS: Germanium, nanowire, silver, gold, nanoparticle, supersaturation, vapor-liquid-solid growth, Gibbs-Thompson effect

Group 14 semiconductor nanowires have a vast range of potential applications, including chemical and biological sensing, computing, optoelectronics and photovoltaic devices.[1-9] High aspect ratio (length vs. diameter) nanowires inherently allow integration of high density device architectures, based on the novel electronic, optical and mechanical properties of nanowires, over large length scales.[10-11] A popular route for growing high aspect ratio one-dimensional (1D) nanostructures is to use a metallic growth promoter in a liquid state, typically gold, as a catalytic seed via a vapor-liquid-solid (VLS) mechanism.[12-15] There are three steps which contribute to nanowire growth kinetics via a VLS mechanism: (i) the incorporation of the growth species from the vapor phase to the liquid growth promoter, (ii) the diffusion of the growth species inside the liquid melt and (iii) crystallization of the growth material at the liquid-solid interface. Steps (i) and (iii) are believed to be key steps in determining the nanowire growth rate.[16-18] Manipulation of the rate determining steps therefore allows the velocity at which nanowires grow to be controlled. To date, research on modifying the growth kinetics of semiconductor nanowires has focused on influencing the concentration of the growth species in the vapor phase, by using high temperatures to induce faster cracking of precursors[19] or by using precursors with higher catalytic decomposition rates.[20-21] However, these methodologies are often restricted by the availability and selectivity of precursors and by the thermodynamically hindered crystallization of growth species at the liquid droplet-solid surface interfaces at high temperatures. According to classical crystal growth theory, growth velocity (v) is proportional to $\left(\frac{\Delta\mu}{kT}\right)^2$, where T is the synthesis temperature and $\Delta\mu$ is a thermodynamic quantity called supersaturation, which is the chemical potential difference between adatoms of growth species in the vapor phase and the solid crystal phase.[17, 22] Supersaturation ($\Delta\mu$) is the driving force in a layer-by-layer crystal growth process where the nucleating islands are formed two-dimensionally (2D) at the triple phase boundary (TPB), followed by a lateral growth process.[23] In reference to the

classical nucleation theory for 2D-island formation, the nucleation rate and the lateral growth rate of islands combine to contribute to the normal growth rate of crystals which have a direct dependence on supersaturation.[24-25] A quadratic dependence of the growth rate of Si nanowires on supersaturation was first reported been by Givargizov.[17] Recently, within a nucleation mediated growth scenario, both linear and quadratic dependences of nanowire growth rates on $\Delta\mu$ have been reported.[18, 26-28] Accordingly, altering the supersaturation will readily influence the growth behavior of nanowires, favoring faster crystallization rates at high $\Delta\mu$ values. Directly influencing $\Delta\mu$ to manipulate the growth rate of nanowires has previously been achieved by altering the partial pressure of the vapor source,[29] according to equation 1 below:

$$P = P_e \, exp(\frac{\triangle \mu}{kT}) \qquad (1)$$

where P_e is equilibrium vapor pressure, k is the Boltzman constant and T the temperature. However, too much of a pressure increase was found to result in escalating sidewall deposition and tapering of Ge nanowires.[29] Using Henry's law, $P_i = \kappa C_i$,where κ is a temperature dependent constant, the magnitude of the concentration (C) of the growth species in a solid or liquid solution can be written in terms of the supersaturation ($\Delta\mu$), the thermal energy of the system (kT) and the equilibrium concentration (C_e) for a bulk system, as shown in equation 2:

$$\triangle \mu = kT \ln(\frac{C}{C_e}) \qquad (2)$$

Hence, increased supersaturation can be achieved by lowering the equilibrium concentration (C_e) of the growth species in the liquid seeds, for a given temperature and precursor

concentration in the vapor phase. A feasible way to manipulate the equilibrium concentration of the growth species along the liquidus phase boundary, to affect $\Delta\mu$, is to incorporate a foreign element into the collector phase, *i.e.* the metal seed particle, which can shift the liquidus phase boundary of the growth species towards a lower solute concentration.

In the synthesis of Group 14 nanowires, via VLS growth, Au has been the collector seed metal of choice due to its low eutectic melting temperature and the high solubility of Group 14 growth species in Au. Lowering the equilibrium concentration (C_e) of the growth species in a liquid collector phase, such as Au, can be achieved by adding a foreign element to the seed, *e.g.* Ag; whilst still maintaining an ideal catalyst system for nanowire growth. The noble metal Ag is readily miscible with Au and they do not form intermetallic compounds or go through a phase change upon dissolution.[30] Both Au and Ag have a simple binary phase diagram with Si or Ge, *i.e.* they do not form "metal-silicide" or "metal-germanide" line compounds, unlike the formation of Cu_3Ge due to the germination of Cu catalyst seeds. Incorporation of one of these metals (Ag or Au) into the other can therefore be used to manipulate the equilibrium growth concentration (C_e) in the eutectic melt at a certain temperature, as alloying the seeds will only effect the position of the liquidus and solidus lines in the binary phase system. Binary phase diagrams[31] of Au-rich Au_xAg_{1-x} alloys with Ge clearly indicate the existence of low eutectic temperatures (~375 - 450 °C), with considerable solubility of Ge near the commonly used nanowire growth temperature (~ 400 °C), using GeH_4 or diphenylgermane (DPG, $(Ph)_2GeH_2$) as Ge precursors in VLS nanowire growth. For example, in a bulk system with Au, Ge forms a eutectic melt at 363 °C with a mole fraction of 0.28 Ge in the alloy, whilst for a $Au_{0.75}Ag_{0.25}$ alloy, Ge has a eutectic temperature of 467 °C and a eutectic composition consisting of Ge at a mole fraction of 0.22.[31] The relatively low eutectic temperature of Au-rich Au_xAg_{1-x} alloys with Ge ensures a reduced growth temperature for efficient VLS nanowire growth, thus minimizing side-wall

deposition and the tapering of nanowires. Normally with a phase pure Au catalyst, Ge nanowire growth is undertaken at a growth temperature close to 400 °C, to enhance cracking of the Ge precursor and hence the generation of long nanowires. However, at approximately 400 °C, the equilibrium concentration of Ge in the metastable eutectic Au-Ge seeds increases considerably (~ 32-33 % for bulk), lowering $\Delta\mu$ and hence hindering nanowire crystallization and growth. With Au_xAg_{1-x} alloy catalysts, the minimal incorporation of Ag into the Au seeds ensures a depression in the Ge equilibrium concentration (C_e) without compromising much on the eutectic temperature, *i.e.* the eutectic temperature only increases slightly, as depicted in the liquidus surface projection of the bulk Au-Ag-Ge ternary phase system.[32] Thus increasing the Ag component in the Au seeds to a certain limit (~20 % at our synthesis temperature of 455 °C), favorably modifies $\Delta\mu$ by decreasing C_e of Ge in the collector seed. Precursor decomposition kinetics can also be driven at increased growth temperatures required for alloy seeded nanowire growth compared to phase pure Au. Eutectic point depression and the change in the Ge liquidus content due to nanosize effects[33] should also be considered for small nanoparticle seeds compared to their bulk counterparts.

In this article, the application of Au-rich ($Au_{0.90}Ag_{0.10}$ and $Au_{0.80}Ag_{0.20}$) colloidal alloy nanoparticles as growth promoters for manipulating the growth kinetics of Ge nanowires via a VLS mechanism is detailed. The successful manipulation of $\Delta\mu$ in Au-Ag-Ge ternary systems influences the induction time and growth rate of Ge nanowires. For the first time, we explore the fundamental insights of thermodynamic manipulation in ternary eutectic systems within the common Gibbs-Thompson framework, taking into account the surface contribution of nanoscale systems. We also detail how changing the composition of the eutectic alloy seed effects the thermodynamically attainable minimum nanowire diameter; *i.e. critical diameter*. Though fundamental investigations on the thermodynamic and kinetic aspects involved in a VLS growth processes is well documented, manipulating them with a simple

innovative alloying approach will open up possibilities for the unlimited growth engineering of nanowires.

Participation of Au_xAg_{1-x} alloy seeds in the bottom-up growth of Si/Ge nanowire heterostructures and super-thin Ge nanowires has previously been demonstrated.[34-35] In this study, dodecanethiol-stabilized phase pure Au and Au-rich ($Au_{0.90}Ag_{0.10}$ and $Au_{0.80}Ag_{0.20}$) alloy nanoparticles were synthesized by co-reducing a mixture of chloroauric acid ($HAuCl_4$) and silver nitrate ($AgNO_3$) in a chloroform/water biphasic solution.[36] Nanoparticles between 2.5-3 nm in diameter were precipitated with ethanol and dispersed in toluene for further use. A single surface plasmon resonance (SPR) peak was observed in the absorbance spectra for all nanoparticle compositions, with a red shift in the SPR peak with increasing Au component in the alloy seeds; confirming the formation of Au_xAg_{1-x} alloy nanoparticles, rather than the growth of core/shell-structured Ag/Au and Au/Ag, or mixtures of Au and Ag, nanoparticles (figure S1, Supporting Information). These small colloidal alloy nanoparticles were deposited onto silicon (001) substrates and dried at 180 °C under vacuum, leading to desorption of the surfactant molecules from the surface of the particles. The native oxide layer on the Si substrates also played a role in pre-alignment the nanoparticles, with respect to the Si lattice, prior to Ge nanowire growth as the fourfold symmetry of a hydrogen-terminated Si (001) surface can force multiple orientation and deviations to Au_xAg_{1-x} (111) particles with threefold symmetry.[37]

A liquid injection chemical vapor deposition (LICVD) technique, using toluene as the solvent phase, was adopted for growing the Ge nanowires on the surface of Si(001) substrates. Diphenylgermane (DPG) was used as the Ge source in the reactions and the nanoparticle concentration in each case was fixed at 40 μmole cm^{-3}. The concentration of DPG in toluene was fixed at 5 μmol ml^{-1}. As anticipated from the phase diagram, the effective growth of Ge

nanowires was achieved from the phase pure gold nanoparticles and Au_xAg_{1-x} alloy nanoparticle seeds ($Au_{0.90}Ag_{0.10}$ and $Au_{0.80}Ag_{0.20}$) after a 45 min growth time, as shown in the scanning electron microscopy (SEM) images in figures 1a, b and c respectively. The Ge nanowire length was observed to increase with a rising concentration of Ag in the nanoparticle seeds. This phenomenon directly relates to the shift in the Ge liquidus phase boundary in the bulk phase diagram, towards lower Ge concentrations, upon incorporation of Ag into the Au-Ge eutectic system (figure 1d). The shift in the Ge equilibrium concentration (C_e) directly effects the supersaturation ($\Delta\mu$) and hence the nucleation probability and crystal growth rate of the Ge nanowires. The participation of the Au_xAg_{1-x} alloy seeds in the growth of the Ge nanowires was confirmed by the energy dispersive x-ray (EDX) analysis performed on the metal tip of the nanowires (Supporting Information, figures S2 and S3). At a synthesis temperature of 455 °C, a reduction in the equilibrium solubility of Ge from approximately 37 to 23 % is likely with a 20 % induction of Ag in the bulk Au_xAg_{1-x} alloy seeds. As the longest nanowires were achieved with the $Au_{0.80}Ag_{0.20}$ growth catalysts, the growth time was significantly increased (to 150 min) with the same seeds to achieve *super-long* Ge nanowires; with lengths between 200 μm to 1.5 mm (see Supporting Information, figure S4). SEM analysis of the nanowire bundles (figures 2a and b) confirmed the growth of millimetre-long Ge nanowires. The superior length of the Ge nanowires is also confirmed by the image shown in figure 2c, with aspect ratios exceeding 5000, without the formation of Ge clusters or other particulate bi-products (figure 2b). X-ray diffraction (XRD) patterns (figure 2d) and high resolution TEM analysis (figure 2e and figure S5) of the *super-long* Ge nanowires exhibited a bulk diamond cubic crystal structure (PDF 04-0545), with a dominant <111> growth direction, with almost 90 % of the nanowires directed along [111] growth axis; the most commonly observed growth orientation in this diameter range.[38-39] The monocrystalline nature of the Ge nanowires, with a 2-4 nm amorphous oxide coating was also confirmed by TEM (see Supporting Information, figure S5). The uniform crystallinity along a100 μm

length of a *super-long* Ge nanowire was verified through lattice-resolved TEM analysis (see Supporting Information, figure S6). *Super-long* nanowires with uniform structural and electronic properties could be appealing for multiple device integration on a single nanowire. These very long nanowires could also facilitate interconnection between arrays of nanoelectronic devices defined on a single nanowire over millimetre length scales.[20]

A time-dependent comparison between Ge nanowires grown from Au and $Au_{0.80}Ag_{0.20}$ alloy seeds revealed that after 30 min Ge nanowires with lengths between 2- 12 μm (inset of Figure 3) were grown from the alloy seeds. However, over the same time period only 100-500 nm long Ge nanowires were produced from the Au seeds (figure 3), implying a slower nucleation and growth rate with the pure metal nanoparticles. After 45 min, Ge nanowires with lengths between 1-6 μm (inset of figure 3) were observed to grow from the Au seeds; whilst nanowires with lengths between 5-20 μm were grown from the alloy seeds at a 45 min growth time (figure 3). Nanowires lengths between 200-600 μm and 50-100 μm were obtained after a growth time of 120 min from $Au_{0.80}Ag_{0.20}$ alloy and pure Au seeds respectively. The collection of SEM images shows Ge nanowire growth after different time intervals and broadly clarifies the participation of different nanowire growth regimes with the Au and $Au_{0.80}Ag_{0.20}$ seeds. The length distributions of the relatively short nanowires (<10 μm) shown in the inset of figure 3 were measured by dark field scanning transmission electron microscopy (STEM), whereas the lengths of long nanowires (> 10 μm) were estimated from SEM analysis.

For an accurate estimation of the different growth kinetics with the three different catalyst systems, nanowires grown after short time interval were considered. A plot of nanowire growth rate distributions with the three different seeds, see figure 4a, clearly shows a fivefold increase in the nanowire growth rate with $Au_{0.80}Ag_{0.20}$ seeds compared to pure Au seeds,

whilst a two fold increase was observed for $Au_{0.90}Ag_{0.10}$ alloy seeds. To calculate the mean lengths and hence the corresponding growth rates from the seeds, nanowires grown from Au_xAg_{1-x} seeds after 30 min were considered (figure S7). Nanowires produced from pure Au seeds were studied after a 45 min growth time (figure S7); as only short and kinked nanowires were observed after a 30 min growth time (figure 3) due to slower growth kinetics. Although the nucleation kinetics of Ge would be different for the three seed types, the incubation time for nanowire growth from all of the nanoparticles would be negligible compared to the reaction times of 30 and 45 min studied here.[40] The rate of incubation involves two time frames: the time required for the precursor to travel from the source chamber to the reaction chamber and then decompose, which would be the same for all three of the eutectic systems investigated. Next, the requisite time for the first nucleation event is predicted to be on the millisecond timescale, hence the difference in timescales for the first nucleation of Ge from the three different seed types is negligible compared to the 30-45 min reaction times. However, in a 2D Layer-by-layer nanowire growth process, the normal growth rate accounts for multiple nucleation events and lateral crystal evolution over the duration of the synthesis. Nucleation is a process of generating a new phase from a metastable old phase, where the Gibbs energy per molecule of the bulk of the emerging new phase is less than that of the solvated old phase. For nanowire growth near the eutectic temperature, where simultaneous multiple nucleation events contribute together towards nanowire growth kinetics, the waiting time for Ge nucleation at the TPB (τ_{Ge}) can therefore be influential. Nucleation time mainly depends on the supersaturation and hence on the composition along the Ge liquidus phase boundary.[41] Ge nanowires grow via 2D nucleation and step propagation at a catalyst/nanowire interface. In a kinetically-limited chemical process, in the context of classical nucleation theory, the rate of nucleation in a condensed system, *i.e.* a liquid-solid system in VLS growth, is proportional to the exponential of the

maximum Gibbs energy necessary for nucleus formation, *i.e.* barrier height (ΔG_b), the Gibbs energy barrier between the old and new phases[42], is shown below in equation 3:

$$P(t) = K \exp(-\Delta G_b / k_b T) \quad (3)$$

where K is a constant dependent on the Zeldovich factor which is a thermodynamic correction factor, monomer concentration and the molecular attachment frequency, T is the temperature and k_b is the Boltzmann constant. The barrier height, ΔG_b, is inversely proportional to the square of the supersaturation ($\Delta\mu$)[43] and the monomer concentration for an ideal solution with a uniform distribution of Ge can be written as a function of $\Delta\mu$ as $C = C_e$ *exp* ($\Delta\mu/k_bT$), where C_{eq} is the equilibrium Ge concentration. As the exponential dependency outgrows the pre-exponential factor, thus for a certain experimental condition, *i.e.* for a fixed temperature, precursor partial pressure *etc*., the general rate of critical nucleation formation from a supersaturated solution is proportional to $exp(a\Delta\mu\text{-}b/\Delta\mu^2)$, where a and b are undetermined constants.[42, 44] The nucleation time (τ_{Ge}) is a reciprocal of nucleation rate $P(t)$, leading to a the direct dependence of the Ge equilibrium concentration on the incubation time as $\Delta\mu$ depends directly on C_e according to equation 2. This relationship provides a clear understanding of how the 2D ledge nucleation of Ge in a layer-by-layer growth process could be affected by tuning the Ge liquidus composition, at a reduced equilibrium concentration of Ge. The enhanced supersaturation with Au_xAg_{1-x} alloy seeds increases the nucleation rate for each step and hence when adding all the nucleation steps together results in an overall faster nanowire growth rate with the Au_xAg_{1-x} alloys. The most important aspect of the overall growth process is the normal crystal growth rate and its dependence on supersaturation. According to classical growth kinetics theory (Givargizov-Chernov (GC) model)[22], the

growth rate (v) has a non-linear dependence on the supersaturation, *i.e.* $v = \mathrm{b}\left(\frac{\Delta\mu}{kT}\right)^2$. For a nanoscopic system having high surface-to-volume ratio the contribution of the surface energy to the thermodynamics is prominent, resulting in a diameter dependent growth rate. Considering the Gibbs-Thompson common framework for VLS growth, the growth rate becomes diameter (d) dependent,[45-47] with a dependence of chemical potential on nanowire diameter, *i.e.* $\Delta\mu = \Delta\mu_0 - \frac{4\Omega\alpha}{d}$, where $\Delta\mu_0$ is the effective difference between the chemical potential of Ge in the vapor phase and in the nanowire, *i.e.* supersaturation, at a plane boundary ($d \rightarrow \infty$), Ω is the atomic volume of Ge, and α is the surface energy. The GC model for nanowire growth and the expression for radial dependent chemical potential clearly indicates a growth rate increment with a decrease in equilibrium concentration of Ge in the metastable phase, as $\Delta\mu \propto ln\left(\frac{C}{C_e}\right)$ for a certain diameter range. The growth rate distribution (figure 4a) explores the effect of Ag inclusion on the thermodynamics of the Au-Ag-Ge eutectic systems, considering the bulk scenario; without taking account of the nanosize effect on the thermodynamic behavior. However, a nanoscale system, due to its enormous surface contribution, will significantly deviate from the bulk phase diagram, effecting the Ge-liquidus concentration.[48] To include this deformation of the phase diagram due to nanoscale influences, the Gibbs-Thompson effect needs to be considered in the nanowire growth rates with phase pure Au and Au_xAg_{1-x} alloy seeds. The Gibbs-Thompson effect readily contributes to the nanowire growth velocity by making it radius dependent[17] as shown in equation 4:

$$v^{1/2} = b^{1/2}\frac{\Delta\mu_0}{kT} - \frac{4\Omega\alpha}{kT}b^{1/2}\frac{1}{d} \qquad (4)$$

where, *b* is the kinetic coefficient of growth at the solid-liquid interface between the nanowire tip and the seed droplet and *d* is the nanowire diameter. Considering the influence of Ge vapor pressure on the diameter of liquid droplet[49] and Henry's law, the diameter dependent second term in equation 4 can be replaced by the equilibrium concentration of Ge at the nanoscale[29], as shown in equation 5:

$$v^{1/2} = b^{1/2}\frac{\Delta\mu_0}{kT} - b^{1/2} ln\left(\frac{C_{nano}}{C_{bulk}}\right) \quad (5)$$

where C_{bulk} and C_{nano} are the bulk and nanoscale equilibrium concentrations, respectively. In this new scenario, apart from the bulk supersaturation ($\Delta\mu_0$), which was controlled by the inclusion of Ag in the Au-Ge binary eutectic alloy, deviations in the Ge equilibrium concentration with nanowire diameter and hence the effect on supersaturation for each nanoscopic system also needs to be considered (2nd term in equation 5). The ratio of C_{nano} and C_{bulk} for each growth system (Au-Ge, $Au_{0.90}Ag_{0.10}$-Ge and $Au_{0.90}Ag_{0.10}$-Ge) determines the shift in Ge-liquidus for a nanoscale system and the impact of the nanosize effect on the growth velocity of the nanowires. How the growth rate of Ge nanowires changes as a function of diameter, for the Au and alloy seeds, is shown in figure 4b. Short growth times (30 and 45 min) yield nanowires with a similar diameter range (figure S8) for all three seeds. Due to lower melting point and hence larger diffusion co-efficient, $Au_{0.80}Ag_{0.20}$ seeds produce nanowires with slightly thicker diameters (mean diameter 48 nm) compared to Au (36 nm) and $Au_{0.80}Ag_{0.20}$ (38 nm) seeds, due to the enhanced diffusion of Au seeds during high temperature growth.[50] To calculate the diameter dependence on the growth rate,

nanowires over a similar diameter range (30-70 nm) were selected from all three systems. A diameter dependent growth rate, obeying the Gibbs-Thompson rule, was observed for all of the VLS-seeded nanowires; an increased growth velocity for larger diameter nanowires followed a quadratic dependence as formulated by Givargizov (GC model).[17] An increased nanowire growth rate (v) was also witnessed for the $Au_{0.80}Ag_{.020}$ and $Au_{0.90}Ag_{.010}$-seeded Ge nanowires, compared to those synthesized from phase pure Au seeds, for the same diameter range. A linear dependence of $v^{1/2}$ with the inverse of diameter ($1/d$) was observed for all of the nanowire growth systems studied, confirming a kinetically driven supersaturation-based growth mechanism as the driving force for nanowire crystallization (figure 4c). According to equation 4, the inclinations of the linear curves, in figure 4c, accounts for the kinetic coefficient and surface energy density of the nanowires. The parallel linear curves with equal slopes imply a minimal effect of the alloying of Au seed particles on the kinetics and energetics at different interfaces during nanowire growth. An increased supersaturation with the alloyed Au_xAg_{1-x} seeds can be inferred from the linear plot (figure 4c), where a gradually increasing intercept cut-off value at the Y-axis ($v^{1/2}$-axis) with increasing Ag concentration in Au-Ag-Ge system (equation 4). The intercept cut-off at the *1/d* axis by extrapolation of the linear fit curve (figure 4c) allows determination of the critical diameter, $d_c = \frac{4\Omega\alpha}{\Delta\mu_0}$, of the Ge nanowires for VLS growth; where for the given overall supersaturation in the vapor phase, actual supersaturation in the seed droplet near the growth interface becomes zero and VLS growth terminates. As indicated in the formulation of d_c, a mechanism to increase the supersaturation will have a favourable effect on lowering the theoretical cut-off diameter for nanowire growth in a VLS mechanism. Increasing supersaturation with alloyed Au seeds lowers the thermodynamically achievable limit of the diameter for VLS-nanowire growth from 9.1 nm for Au-seeded growth to 5.5 nm for $Au_{0.80}Ag_{0.20}$ alloy-seeded growth at 455 °C, whilst a *critical diameter* of 6.9 nm was obtained for $Au_{0.90}Ag_{0.10}$-seeded growth (figure 4d).

Narrowing and/or tuning the *critical diameter* of VLS-grown nanowires paves the way to extend their radial limit towards the atomic scale. Fabrication of extremely small diameter-one-dimensional nanostructures leads to strong carrier confinement and energy quantization, or even a complete energy band restructuring.[51] However, due to strong inter-particle diffusion, nanowires with much larger diameters than the thermodynamic limit were synthesized. Also, from the linear fit of equation 4 (figure 4c) and using a Ge atomic volume (Ω) of 2.26×10^{-23} cm^3 and a surface energy (α) of 0.88×10^{-4} J cm^{-2},[52] values of $\Delta\mu_0$ were determined from the critical diameter formulation. The bulk supersaturation values increased gradually from 54.5 (x = 1) to 90.2 meV (x = 0.8), with the increasing Ag content in the Au_xAg_{1-x} alloys (figure 4d). All of the arguments above are based on the assumption that the nucleation-mediated layer-by-layer growth mode obeys the Gibbs-Thompson effect. As modelled before,[53] with a modest concentration of source in the vapour phase (as in our synthetic condition, 5 μmole cm^{-3} of DPG) , nucleation-mediated growth processes at the liquid-surface interface remain dominating, showing a pronounced Gibbs-Thompson effect. Whereas at a large precursor vapor concentration, a diffusion driven adsorption-desorption process controls the nanowire growth process.

The involvement of supersaturation-driven growth kinetics and the influence of equilibrium concentration was further observed by *in-situ* annealing experiments inside a TEM.[54-55] The diameter dependent melting of metal seeds at the tips of Ge nanowires was observed in-situ. The change in the volume of Au-Ge and Au-Ag-Ge alloy liquid droplets as a function of temperature, for different diameter nanowires, was measured allowing the equilibrium compositions of Ge in the various eutectic melts to be determined.[56] Since all three eutectic systems (Au-Ge, $Au_{0.90}Ag_{0.10}$-Ge, and $Au_{0.80}Ag_{0.20}$-Ge) have spatial dimensions in the nanometer range, excess energies due to free surfaces and interfaces can no longer be

neglected but become comparable to the "bulk" contributions to the total Gibbs energy. Hence, a significant alteration in the equilibrium Ge concentration in the metal-tip of the nanowires is expected with different diameter nanowires which results in diameter dependent growth kinetics. This behaviour is directly related to the concentration dependent 2nd term of equation 5, where the variation in the Ge equilibrium concentration of nanosize eutectics (C_{nano}) will readily modify the growth rate compared to their bulk counterparts. The *in-situ* TEM heating experiments with different diameter nanowires for all three different eutectic systems showed a direct demonstration of the size-dependent liquidus Ge concentration. Figures 5a-c show the evolution of nanowire shape with Au, $Au_{0.90}Ag_{0.80}$, and $Au_{0.80}Ag_{0.20}$ droplets at the nanowire tips during the heat treatment from room temperature to 455 °C. Surface melting of eutectic droplets followed by melting of entire nanoparticles close to the respective bulk eutectic temperature (T_e), with an uptake of Ge from the nanowires was observed for all three eutectic systems. Above the eutectic temperature the metal droplets at the tip became liquid. A further increase in temperature to 455 °C forces a gradual expansion in the liquid drop, due to an increase in the Ge content in the eutectic alloys. These observations were recorded for different diameter nanowires with Au-Ge binary and Au-Ag-Ge ternary eutectic alloys. To quantify the Ge content in the binary and ternary eutectic alloys at elevated temperatures, data from drop volume measurements[48] were used to relate the Ge content in the alloys at equilibrium. The diameter dependent Ge contents at 455 °C in the Au-Ge, $Au_{0.90}Ag_{0.10}$-Ge, and $Au_{0.80}Ag_{0.20}$-Ge eutectic alloys for different nanowire diameters are shown in figure 5d. The experimental data agrees well with the theoretical fit based on the Gibbs-Thompson effect, $C_{nano} = C_{bulk}\, exp(\kappa 4\Omega\alpha_{Ge}/dkT)$, where κ is a constant which accounts for changes in the drop shape.[29] For all three of the eutectic alloys considered, the equilibrium Ge content decreased with an incremental amount of Ag in the eutectic composition. Also, an upward trend in the Ge content as a function of decreasing nanowire diameter was evident for all of the eutectic systems. Consideration of the

concentration dependent term in equation 5, data obtained from the *in-situ* TEM heating experiments were readily linked to the nanowire growth kinetics (figures 4b and c). Using the proper fitting factors (κ = 2.3 to 2.4) and bulk supersaturation values ($\Delta\mu_0$) obtained from the growth rate experiment, the diameter (d) dependence of the supersaturation ($\Delta\mu$) was plotted for all three growth systems used. The linear dependence of $\Delta\mu$ with 1/d for nanowire growth with all three catalytic systems agrees with the Gibbs-Thompson model (figure 5e). The parallel plots confirm similar kinetics and energetics at different interfaces during nanowire growth with all three catalyst systems. The Y-axis intercept of the linear fitted curve of $\Delta\mu$ vs 1/d portrays the bulk values of Ge supersaturation for all three nanoparticle seeds at our growth conditions. The supersaturation increased from 52.1 to 84.9 meV with a decrease in *critical diameter* from 13 to 7.2 nm for the binary Au-Ge alloy compared to the ternary $Au_{0.80}Ag_{0.20}$-Ge alloy, respectively, advocating the enhanced nanowire growth kinetics observed with the alloy seeds in the supersaturation limited growth process. Considering the binary Au-Ge system, lowering of the Ge equilibrium concentration at low temperatures in the eutectic regime can result in higher supersaturation and faster crystal growth. But lowering the growth temperature to achieve faster crystallization at the TPB could have an adverse effect on the nucleation and precursor decomposition kinetics and thus on the overall nanowire growth rate. Also, increasing the feed rate of reactants could increase the nanowire growth rate, but not without sidewall deposition (resulting in large diamter nanowires) and the formation of particulate bi-products (figure S9). In contrast, the novel methodology discussed in this article, with ternary eutectic systems may have universal applicability in nanowire growth engineering and could be applied to different potential "seed material-nanowire" systems, especially for Group 14 nanowires. For example, collector seed materials with low Ge or Si solubility, *type B*, could be incorporated into Au seeds to significantly lower the equilibrium concentration of the growth material (Ge or Si) which will have an immediate effect on the nucleation and growth kinetics.

In summary, a new approach for controlling the growth behavior of Ge nanowires via a bottom-up VLS approach, employing Au_xAg_{1-x} alloy seeds, has been demonstrated. Varying compositions of the Au_xAg_{1-x} alloys facilitated the manipulation of thermodynamic growth limiting factors to produce favorable growth environments for long nanowires, successfully resulting in millimetre-long Ge nanowires for potential multiple device integration. Enhanced supersaturation with decreasing equilibrium Ge concentration in the alloy seeds enabled a lowering of the limit of radial dimension in VLS nanowire growth, *i.e.* the *critical diameter*. The demonstration of the Gibbs-Thompson effect for the growth of Ge nanowires from ternary alloys opens up enormous research opportunity to look into the fundamental insights; *i.e.* thermodynamics and kinetics, of nanoscale phenomenon with ternary eutectic alloys which has been limited to mainly Au-Ge system up to now. Keeping in mind the large amount of possible metal alloy combinations which can act as growth promoters for group 14 and 13-15 nanowires, VLS-nanowire growth with ternary eutectic systems has the potential to revolutionize nanowire growth engineering. This new approach of manipulating the supersaturation by changing the equilibrium solubility of the solute growth material in a liquid-seeded growth approach, could be combined with other critical growth constraints, *i.e.* pressure, temperature, dopant concentration, precursor decomposition chemistry *etc*. to realize a perfect scenario for much improved growth engineering in nanowires.

Methods: A colloidal dispersion of seed nanoparticles with different Au and Ag ratios were synthesized by varying the molarity of the Au^+ and Ag^+. Dodecanethiol (DDT)-stabilized nanoparticles were prepared in chloroform using tetra-octyl amino bromide (TOAB), $(C_8H_{17})_4NBr$), as a phase transfer catalyst and an aqueous sodium borohydride solution (~0.44 M), $NaBH_4$, as the reducing agent. The organic phase was separated and precipitated

with ethanol. The precipitation was cleaned with ethanol and redispersed in toluene for further use as catalyst in nanowire growth.

Continuous-flow reactions for nanowire growth were carried out in a toluene medium using a liquid-injection chemical vapor deposition (LICVD) technique. Metal nanoparticles were spin-coated onto a Si (001) substrate and loaded into a stainless steel micro reactor cell, connected to metal tubing. The reaction cell and connections were dried for 24 h at 180 °C under vacuum. Solutions of diphenylgermane (DPG), the Ge precursor, in anhydrous toluene were prepared in an N_2 glove box with a typical concentration of 5 μmole ml^{-1}. A DPG solution (5 μmole ml^{-1}) was loaded into a Hamilton sample-lock syringe inside a nitrogen-filled glovebox. Prior to injection, the coated Si substrate was annealed for 15 min at 455 ºC under a flowing H_2/Ar atmosphere inside a tube furnace. The precursor solution was then injected into the metal reaction cell using a high pressure syringe pump at a rate of 0.025 ml min^{-1}. A H_2/Ar flow rate of 0.5 ml min^{-1} was maintained during the entire growth period. Typical growth times were varied to study the effect on nanowire length. The reaction cell was allowed to cool to room temperature and disassembled to access the growth substrate. Nanowires were washed with dry toluene and dried under N_2 flow for further characterization.

To measure the length of the nanowires dark filed scanning transmission electron microscopy (STEM) technique was used. Ge Nanowires were transferred from the Si substrate to a carbon coated Cu-grid using a dry transfer technique. Nanowires were scraped from Si substrate and dropped down onto a carbon coated grid. To measure the length and growth rate only short (< 10 μm) nanowires were considered, as bending for longer wires could result in error in the length measurements.

The one-dimensional Ge nanostructures were analyzed using a FEI quanta 650 scanning electron microscope (SEM) and a JEOL 2100 transmission electron microscope (TEM) operated at 200 kV equipped with an EDX detector (Oxford Instruments INCA energy system). Length measurements were performed using dark field scanning transmission electron microscopy; carried out on a FEI Helios Nanolab^{TM} dual-beam SEM suite operating at 5 kV. X-ray diffraction (XRD) studies were performed on a Phillips Xpert diffractometer. The TEM heating experiments were performed on a JEOL 2100 TEM equipped with a Gatan 652 high-temperature sample holder.

ACKNOWLEDGEMENTS

We acknowledge financial support from Science Foundation Ireland (Grant: 09/IN.1/I2602). This research was also enabled by the Higher Education Authority Program for Research in Third Level Institutions (2007-2011) via the INSPIRE programme.

ASSOCIATED CONTENT

Supporting Information. Detail of nanoparticles including TEM images and absorbance spectra, EDX studies and TEM images of the synthesized Ge nanowires and nanoparticle seeds, statistical data on nanowire diameters, results for nanowire growth with higher precursor flux. This material is available free of charge via the Internet at http://pubs.acs.org.

References:

1. Burchhart, T.; Zeiner, C.; Lugstein, A.; Henkel, C.;Bertagnolli, E. Tuning the Electrical Performance of Ge Nanowire Mosfets by Focused Ion Beam Implantation. *Nanotechnology* **2011,** *22*, 035201.
2. Garnett, E.;Yang, P. D. Light Trapping in Silicon Nanowire Solar Cells. *Nano Lett.* **2010,** *10*, 1082-1087.
3. He, R. R.; Gao, D.; Fan, R.; Hochbaum, A. I.; Carraro, C.; Maboudian, R.;Yang, P. D. Si Nanowire Bridges in Microtrenches: Integration of Growth into Device Fabrication. *Advanced Materials* **2005,** *17*, 2098-+.
4. Leonard, F.; Talin, A. A.; Swartzentruber, B. S.;Picraux, S. T. Diameter-Dependent Electronic Transport Properties of Au-Catalyst/Ge-Nanowire Schottky Diodes. *Physical review letters* **2009,** *102*, 106805.
5. Liu, Y.-C. C.; Rieben, N.; Iversen, L.; Sorensen, B. S.; Park, J.; Nygard, J.;Martinez, K. L. Specific and Reversible Immobilization of Histidine-Tagged Proteins on Functionalized Silicon Nanowires. *Nanotechnology* **2010,** *21*.
6. Seo, M. H.; Park, M.; Lee, K. T.; Kim, K.; Kim, J.;Cho, J. High Performance Ge Nanowire Anode Sheathed with Carbon for Lithium Rechargeable Batteries. *Energy Environ. Sci.* **2011,** *4*, 425-428.
7. Wu, X. Y.; Kulkarni, J. S.; Collins, G.; Petkov, N.; Almecija, D.; Boland, J. J.; Erts, D.;Holmes, J. D. Synthesis and Electrical and Mechanical Properties of Silicon and Germanium Nanowires. *Chem. Mat.* **2008,** *20*, 5954-5967.
8. Xiang, J.; Lu, W.; Hu, Y. J.; Wu, Y.; Yan, H.;Lieber, C. M. Ge/Si Nanowire Heterostructures as High-Performance Field-Effect Transistors. *Nature* **2006,** *441*, 489-493.
9. Yi, K. S.; Trivedi, K.; Floresca, H. C.; Yuk, H.; Hu, W.;Kim, M. J. Room-Temperature Quantum Confinement Effects in Transport Properties of Ultrathin Si Nanowire Field-Effect Transistors. *Nano Lett.* **2011,** *11*, 5465-5470.
10. Cui, Y.;Lieber, C. M. Functional Nanoscale Electronic Devices Assembled Using Silicon Nanowire Building Blocks. *Science* **2001,** *291*, 851-853.
11. Duan, X. F.; Huang, Y.; Agarwal, R.;Lieber, C. M. Single-Nanowire Electrically Driven Lasers. *Nature* **2003,** *421*, 241-245.
12. Collins, G.; Kolesnik, M.; Krstic, V.;Holmes, J. D. Germanium Nanowire Synthesis from Fluorothiolate-Capped Gold Nanoparticles in Supercritical Carbon Dioxide. *Chem. Mat.* **2010,** *22*, 5235-5243.
13. Morales, A. M.;Lieber, C. M. A Laser Ablation Method for the Synthesis of Crystalline Semiconductor Nanowires. *Science* **1998,** *279*, 208-211.
14. Barth, S.; Kazakova, O.; Estrade, S.; Hobbs, R. G.; Peiro, F.; Morris, M. A.;Holmes, J. D. Synthesis and Magnetic Characterization of Coaxial Ge1-Xmnx/a-Si Heterostructures. *Crystal Growth & Design* **2011,** *11*, 5253-5259.
15. Adhikari, H.; Marshall, A. F.; Goldthorpe, I. A.; Chidsey, C. E. D.;McIntyre, P. C. Metastability of Au-Ge Liquid Nanocatalysts: Ge Vapor-Liquid-Solid Nanowire Growth Far Below the Bulk Eutectic Temperature. *ACS Nano* **2007,** *1*, 415-422.
16. Bootsma, G. A.;Gassen, H. J. Quantitative Study on Growth of Silicon Whiskers from Silane and Germanium Whiskers from Germane. *Journal of Crystal Growth* **1971,** *10*, 223-&.
17. Givargizov, E. I. Fundamental Aspects of Vls Growth. *Journal of Crystal Growth* **1975,** *31*, 20-30.
18. Schmidt, V.; Senz, S.;Goesele, U. Diameter Dependence of the Growth Velocity of Silicon Nanowires Synthesized Via the Vapor-Liquid-Solid Mechanism. *Physical Review B* **2007,** *75*.
19. Shi, W. S.; Peng, H. Y.; Zheng, Y. F.; Wang, N.; Shang, N. G.; Pan, Z. W.; Lee, C. S.;Lee, S. T. Synthesis of Large Areas of Highly Oriented, Very Long Silicon Nanowires. *Advanced Materials* **2000,** *12*, 1343-1345.
20. Park, W. I.; Zheng, G.; Jiang, X.; Tian, B.;Lieber, C. M. Controlled Synthesis of Millimeter-Long Silicon Nanowires with Uniform Electronic Properties. *Nano Lett.* **2008,** *8*, 3004-3009.

21. Yang, H.-J.;Tuan, H.-Y. High-Yield, High-Throughput Synthesis of Germanium Nanowires by Metal-Organic Chemical Vapor Deposition and Their Functionalization and Applications. *J. Mater. Chem.* **2012,** *22*, 2215-2225.
22. Givargizov, E. I. *Highly Anisotropic Crystals*. Springer:New York: 1987; Vol. Chapter 2.
23. B Lewis;Anderson, J. S. *Nucleation and Growth of Thin Films*. Academic, New York: 1978.
24. Kukushkin, S. A.;Osipov, A. V. New Phase Formation on Solid Surfaces and Thin Film Condensation. *Progress in Surface Science* **1996,** *51*, 1-107.
25. Hurle, D. T. J. *Handbook of Crystal Growth*. Elsevier: Amsterdam, 1994; Vol. 2.
26. Dubrovskii, V. G.;Sibirev, N. V. Growth Rate of a Crystal Facet of Arbitrary Size and Growth Kinetics of Vertical Nanowires. *Physical Review E* **2004,** *70*.
27. Kashchiev, D. Dependence of the Growth Rate of Nanowires on the Nanowire Diameter. *Crystal Growth & Design* **2006,** *6*, 1154-1156.
28. Schmidt, V.; Wittemann, J. V.; Senz, S.;Goesele, U. Silicon Nanowires: A Review on Aspects of Their Growth and Their Electrical Properties. *Advanced Materials* **2009,** *21*, 2681-2702.
29. Dayeh, S. A.;Picraux, S. T. Direct Observation of Nanoscale Size Effects in Ge Semiconductor Nanowire Growth. *Nano Lett.* **2010,** *10*, 4032-4039.
30. Hassam, S.; Agren, J.; Gauneescard, M.;Bros, J. P. The Ag-Au-Si System - Experimental and Calculated Phase-Diagram. *Metallurgical Transactions a-Physical Metallurgy and Materials Science* **1990,** *21*, 1877-1884.
31. Wang, J.; Liu, Y. J.; Tang, C. V.; Liu, L. B.; Zhou, H. Y.;Jin, Z. P. Thermodynamic Description of the Au-Ag-Ge Ternary System. *Thermochimica Acta* **2011,** *512*, 240-246.
32. A Prince, P. L., O Fabrichnaya *Springer Materials the Landotl-Bornstein New Series Iv/Iib*. Springer: 2012.
33. Schwalbach, E. J.;Voorhees, P. W. Phase Equilibrium and Nucleation in Vls-Grown Nanowires. *Nano Lett.* **2008,** *8*, 3739-3745.
34. Biswas, S.; Singha, A.; Morris, M. A.;Holmes, J. D. Inherent Control of Growth, Morphology, and Defect Formation in Germanium Nanowires. *Nano Lett.* **2012,** *12*, 5654-5663.
35. Yi-Chia Chou, C. Y. W., Mark C. Reuter, Dong Su, Eric A. Stach and Frances M. Ross *ACS Nano* **2012**.
36. He, S. T.; Xie, S. S.; Yao, J. N.; Gao, H. J.;Pang, S. J. Self-Assembled Two-Dimensional Superlattice of Au-Ag Alloy Nanocrystals. *Applied Physics Letters* **2002,** *81*, 150-152.
37. Li, B. Q.;Zuo, J. M. Structure and Shape Transformation from Multiply Twinned Particles to Epitaxial Nanocrystals: Importance of Interface on the Structure of Ag Nanoparticles. *Physical Review B* **2005,** *72*.
38. Wu, Y.; Cui, Y.; Huynh, L.; Barrelet, C. J.; Bell, D. C.;Lieber, C. M. Controlled Growth and Structures of Molecular-Scale Silicon Nanowires. *Nano Lett.* **2004,** *4*, 433-436.
39. Schmidt, V.; Senz, S.;Gosele, U. Diameter-Dependent Growth Direction of Epitaxial Silicon Nanowires. *Nano Lett.* **2005,** *5*, 931-935.
40. Eisenhawer, B.; Sivakov, V.; Christiansen, S.;Falk, F. A Time-Resolved Numerical Study of the Vapor–Liquid–Solid Growth Kinetics Describing the Initial Nucleation Phase as Well as Pulsed Deposition Processes. *Nano Letters* **2013,** *13*, 873-883.
41. B J Kim, C. Y. W., J Tersoff, M C Reuter, E A Stach, F M Ross *Nano Lett.* **2012,** *12*, 5867.
42. Turnbull, D.;Fisher, J. C. Rate of Nucleation in Condensed Systems. *Journal of Chemical Physics* **1949,** *17*, 71-73.
43. Neilsen, A. E. *Kinetics of Precipitation*. Pergamon,Oxford: 1964.
44. Gamalski, A. D.; Ducati, C.;Hofmann, S. Cyclic Supersaturation and Triple Phase Boundary Dynamics in Germanium Nanowire Growth. *Journal of Physical Chemistry C* **2011,** *115*, 4413-4417.
45. Weyher, J. Some Notes on Growth Kinetics and Morphology of Vls Silicon-Crystals Grown with Platinum and Gold as Liquid-Forming Agents. *Journal of Crystal Growth* **1978,** *43*, 235-244.
46. Kikkawa, J.; Ohno, Y.;Takeda, S. Growth Rate of Silicon Nanowires. *Applied Physics Letters* **2005,** *86*.
47. Wu, Y. Y.; Fan, R.;Yang, P. D. Block-by-Block Growth of Single-Crystalline Si/Sige Superlattice Nanowires. *Nano Lett.* **2002,** *2*, 83-86.
48. Sutter, E. A.;Sutter, P. W. Size-Dependent Phase Diagram of Nanoscale Alloy Drops Used in Vapor-Liquid-Solid Growth of Semiconductor Nanowires. *ACS Nano* **2010,** *4*, 4943-4947.

49. Froberg, L. E.; Seifert, W.;Johansson, J. Diameter-Dependent Growth Rate of Inas Nanowires. *Physical Review B* **2007,** *76*.
50. Nichols, F. A. Coalescence of 2 Spheres by Surface Diffusion. *Journal of Applied Physics* **1966,** *37*, 2805-&.
51. Jing, M. W.; Ni, M.; Song, W.; Lu, J.; Gao, Z. X.; Lai, L.; Mei, W. N.; Yu, D. P.; Ye, H. Q.;Wang, L. Anisotropic and Passivation-Dependent Quantum Confinement Effects in Germanium Nanowires: A Comparison with Silicon Nanowires. *Journal of Physical Chemistry B* **2006,** *110*, 18332-18337.
52. Jiang, Q.; Lu, H. M.;Zhao, M. Modelling of Surface Energies of Elemental Crystals. *Journal of Physics-Condensed Matter* **2004,** *16*, 521-530.
53. Dubrovskii, V. G.; Sibirev, N. V.; Cirlin, G. E.; Harmand, J. C.;Ustinov, V. M. Theoretical Analysis of the Vapor-Liquid-Solid Mechanism of Nanowire Growth During Molecular Beam Epitaxy. *Physical Review E* **2006,** *73*.
54. Kodambaka, S.; Tersoff, J.; Reuter, M. C.;Ross, F. M. Germanium Nanowire Growth Below the Eutectic Temperature. *Science* **2007,** *316*, 729-732.
55. Kim, B. J.; Tersoff, J.; Kodambaka, S.; Reuter, M. C.; Stach, E. A.;Ross, F. M. Kinetics of Individual Nucleation Events Observed in Nanoscale Vapor-Liquid-Solid Growth. *Science* **2008,** *322*, 1070-1073.
56. Sutter, E.;Sutter, P. Phase Diagram of Nanoscale Alloy Particles Used for Vapor-Liquid-Solid Growth of Semiconductor Nanowires. *Nano Lett.* **2008,** *8*, 411-414.

Figures

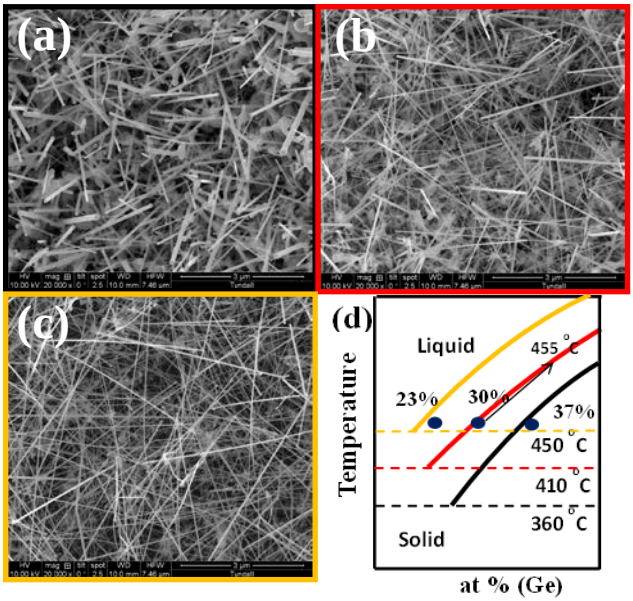

Figure 1 SEM images showing different lengths of nanowires observed with (a) $Au_{0.80}Ag_{0.20}$ (b) $Au_{0.90}Ag_{0.10}$ alloy seeds and (c) phase pure Au seed particles after 45 min of growth . Part (d) shows partial bulk phase diagram depicting the variation in equilibrium Ge concentration along the bulk Ge liquidus for three different catalyst – Ge growth systems ($Au_{0.80}Ag_{0.20}$- Ge (yellow), $Au_{0.90}Ag_{0.10}$ – Ge (red), Au- Ge (black), and blue dots denote synthesis temperature). Phase diagrams are adapted from reference 32.

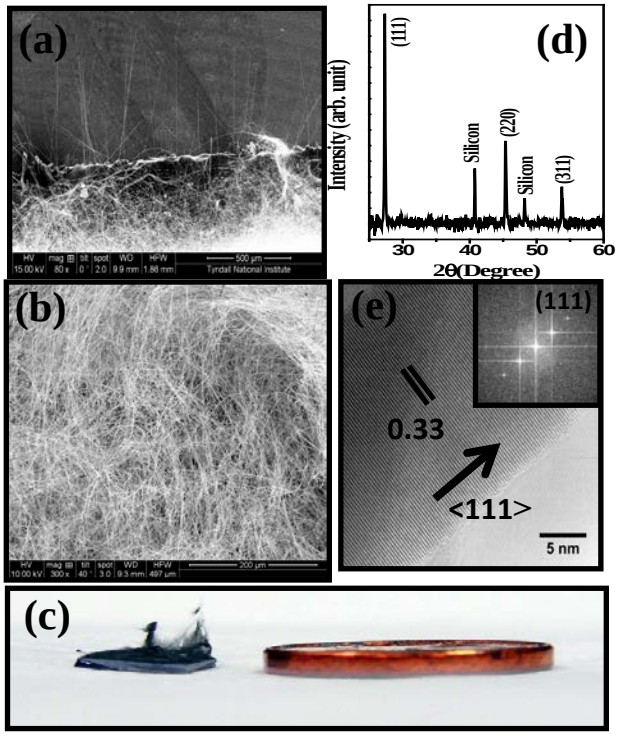

Figure 2. Growth of super-long nanowires is shown in the SEM images in part (a) and (b). Photograph in part (c) confirms high yield and growth of super-long nanowires with a comparison of nanowire length with a Euro cent coin. XRD pattern (part (d)) and TEM image (part (e)) confirm the formation of single crystalline nanowire with Ge fcc symmetry.

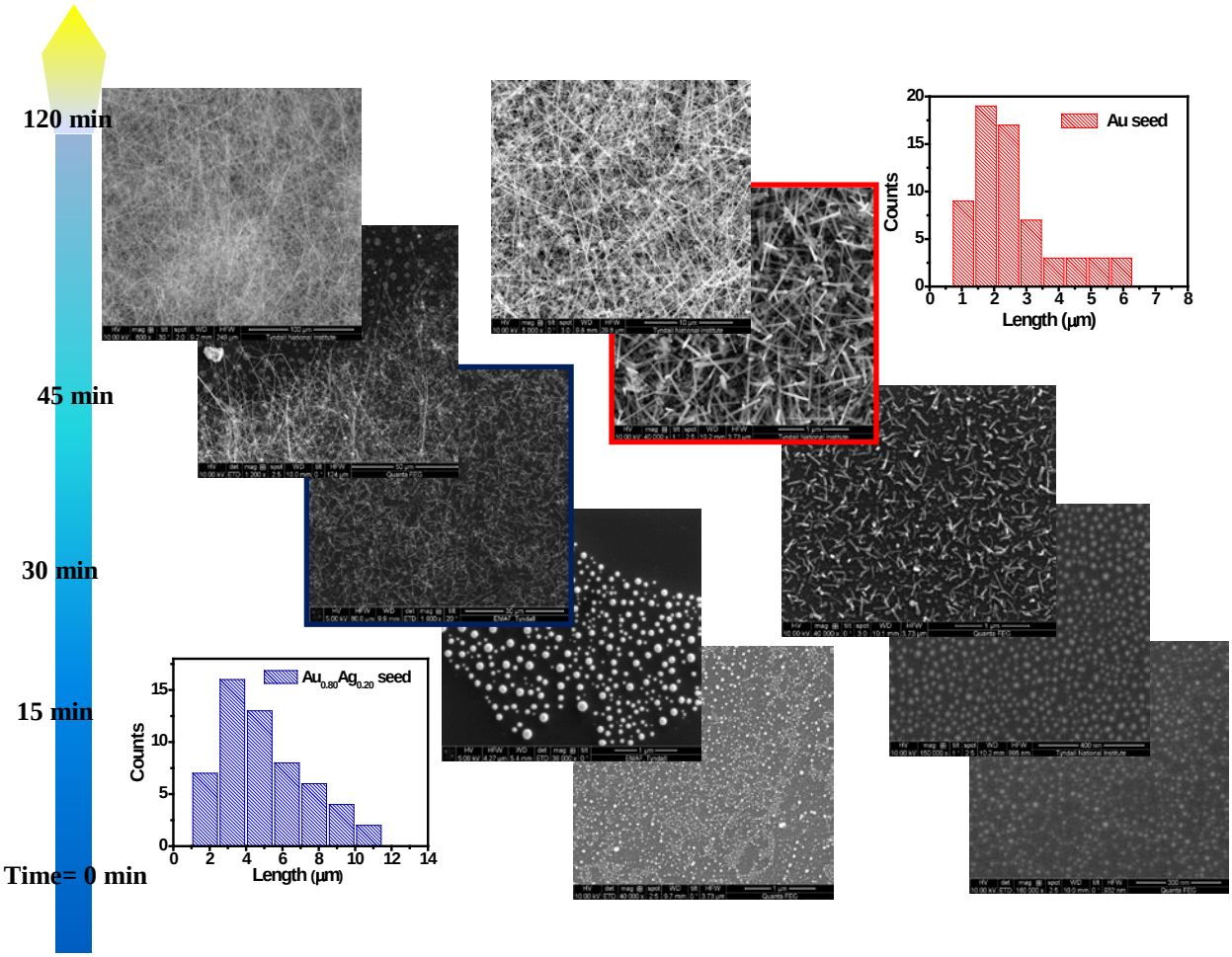

Figure 3. SEM images showing different nanowire growth rates for Au seed and $Au_{0.80}Ag_{0.20}$ alloy seeds. Growth time 0 min signifies 15 min pre-annealing step just before precursor injection. No nanowire growth after 15 min is associated with the time for precursor injection flow from source to reaction chamber. Length distributions of nanowires after 30 min growth from alloy seed and 45 min growth from Au seed are shown in the insets.

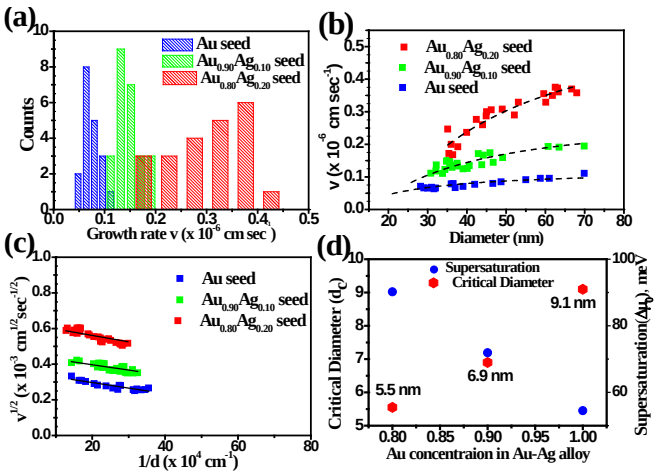

Figure 4. (a) Growth rate distributions with different catalyst systems showing the highest Ge nanowire growth rate with $Au_{0.80}Ag_{0.20}$-Ge seeds. Plots in part (b) show the quadratic dependence of the growth rate with nanowire diameter grown with three different seeds, (c) plots of the square root of the growth velocity showing the linear dependence with inverse diameter, agreeing well with Gibbs-Thompson effect. Part (d) shows the gradual decrease in the *critical diameter* of Ge nanowires and an increase in the supersaturation with Ag incorporation in the Au seed.

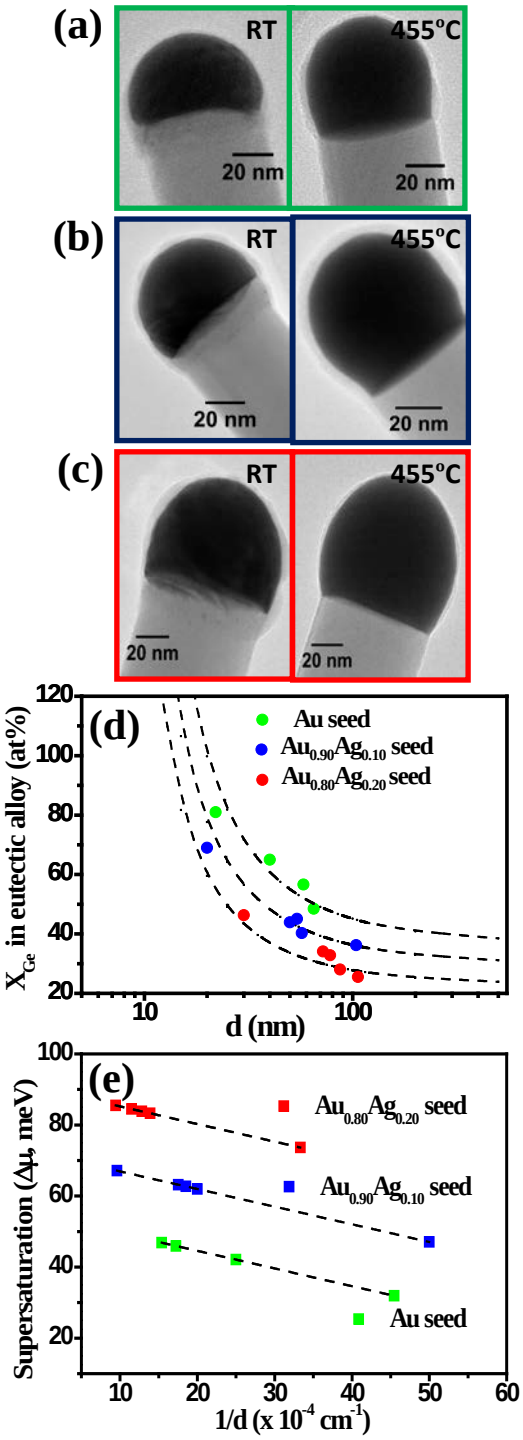

Figure 5. TEM images showing melting and expansion of metal seeds at the tip of Ge nanowire at 455 ºC upon Ge uptake for: (a) Au-Ge, (b) $Au_{0.90}Ag_{0.10}$-Ge and (c) $Au_{0.80}Ag_{0.20}$-Ge eutectic phases. (d) shows Ge atomic % in the eutectic melt as a function of nanowire diameter for different Ag incorporation in the alloy seeds (symbols are experimental data point; dashed lines are fits according to Gibbs-Thompson effect). Parallel linear plots in part (e) shows varying supersaturation with diameter for three different catalyst systems.